Testing of a small Water Resistojet Thruster in Zero-G flight experimental campaign

Fabiano Perini, Stéphane Mazouffre, Guillaume Largeau

Testing of a small Water Resistojet Thruster in Zero-G flight experimental campaign

IEPC-2024-485

Presented at the 38th International Electric Propulsion Conference, Toulouse, France
June 23-28, 2024

Fabiano Perini* and Stéphane Mazouffre† and Guillaume Largeau‡
ICARE (CNRS), Orléans, Loiret, 45100, France

The rapid increase in the number of satellites in orbit, coupled with the growing complexity of their missions and the high risk of collisions, underscores the urgent need for low-cost, compact, reliable, and high-thrust onboard propulsion systems. Traditionally, cold gas nitrogen systems have been favored for their simplicity, combining high reliability with low cost. However, these systems suffer from low specific impulse and poor storage densities. An alternative propellant of interest is pure water. Water is inexpensive, non-toxic, and can be stored in liquid form. Its abundance in the solar system and its low molecular mass enable a high specific impulse. However, there are drawbacks: the water must be very pure, it must be kept from freezing, and additional power is required for vaporization. Finding cost-effective, easy-to-handle propellants is crucial for space agencies and private enterprises worldwide. While traditional systems and advanced options like krypton and xenon have their merits and drawbacks, water emerges as a promising candidate despite its storage and handling challenges. As the quest for green propellant continues, water potential benefits make it an attractive area for further research and development. A small electrothermal water-fueled propulsion thruster was developed and tested at the ICARE laboratory in France. The thruster comprised a spherical tank for liquid water and pressurized gas (air), two printed electronic circuit boards based on the Arduino Nano microcontroller, a vaporization chamber, and a convergent-divergent nozzle for expanding the vapor. The input power remained below 100 W with a scalable thrust in the mN range and a specific impulse below 100 s. Due to the different behavior of liquids in the absence of gravity, the thruster was tested in a zero-gravity flight campaign March 2024. The purpose of the experiments was to compare the performance on the ground with that in a weightless condition. The experimental flight campaign (VP177) was organized by the NoveSpace company in Bordeaux with the AirZeroG airplane. To the best of our knowledge, it was the first time a water-fed Resistojet was operated in a vacuum chamber during a 0-g flight. In this contribution, we shall present the architecture of the water-fueled resistojet and characteristics obtained in microgravity flight experiments. Details about the vaporization chamber will be given as it is a critical component of the propulsion system. Indeed, in the absence of gravity, vaporization must be effective to avoid droplet formation during the expansion process, therefore ensuring high performance.

*Electric Propulsion Engineer, ICARE (CNRS), fabiano.perini@cnrs-orleans.fr.
†Assistant Research Director, ICARE (CNRS), stephane.mazouffre@cnrs-orleans.fr.
‡Electric Propulsion Engineer, ICARE (CNRS), guillaume.largeau@cnrs-orleans.fr.

Nomenclature

$\dot{m}$	= mass flow rate
T_{wall}	= wall temperature
A_l	= area of liquid
T_{sat}	= saturation temperature x direction
P_{vap}	= vaporization power
h_{BO}	= boiling heat transfer coefficient
h_{vl}	= latent heat of vaporization
P_{cond}	= conductive power loss
P_{rad}	= radiative power loss
$P_{superheat}$	= superheating power
p_{vc}	= vaporization chamber pressure
p_{inlet}	= nozzle inlet pressure
Δp_{loss}	= pressure loss
$i(t)$	= current in the heaters
$R_{parallel}$	= Parallel resistence

I. Introduction

The use of liquid water as a propellant for satellites represents an innovative and sustainable solution in the field of space propulsion. Water, which is abundant in our solar system and readily available, offers numerous advantages over traditional propellants. Firstly, it is safe and non-toxic, reducing the risks associated with handling and storage. In addition, water can be easily dissociated into hydrogen and oxygen through electrolysis, offering an on-board hybrid thruster that allows for high thrust or high specific impulse when required. Another significant benefit of water as a propellant is the possibility of using space resources. For example, water can be extracted from ice on the Moon or from asteroids, paving the way for a new era of refuelling and sustainability in space.

Water can be stored in liquid form at atmospheric pressure, reducing the weight of the tank compared to gaseous propellants, which must be stored at high pressure. The water molecule is relatively light; with a molecular weight of 18, it allows for a high specific impulse. However, water also has some downsides. In orbit, the tank must be kept at an adequate temperature to prevent the liquid water from freezing. In addition, to be used as propellant, water must be converted into vapor, which requires a non-negligible amount of energy.

A resistojet thruster is the simplest type of electrothermal thruster in the field of electric propulsion. In this type of device, the liquid propellant is vaporized in a dedicated chamber, the so called vaporization chamber, prior to expansion in a de Laval nozzle.

Since the propellant is liquid, gravity plays a crucial role, so certain measures must be taken: if the liquid water is not completely vaporized and reaches the nozzle in liquid state, thruster performance may degrade, potentially leading to a complete stall. Therefore, it is essential to design the vaporization chamber so that it completely vaporises the propellant and ensures high vaporization efficiency. The boiling process is highly dependent on gravity, so it is necessary to test the thruster under weightless conditions to characterise its true performance and verify any differences from those measured a in laboratory.

An economical method to test the thruster in microgravity is to conduct experiments in a drop tower. However, this approach has disadvantages: the drop time is typically very short, around 1-2 seconds, and there are spatial constraints. Consequently, a parabolic flight is preferable for accurately measuring performance over a longer duration.

Over the past year, at the ICARE laboratories of the CNRS in Orléans (France), a prototype water resistojet has been fabricated, and the entire experiment for the zero-g flight has been prepared from scratch. The experiment has been selected in the CNES parabolic flight campaign (VP177). Numerous challenges were encountered due the stringent safety restrictions imposed by the organization conducting the experimental flights. Therefore, it was necessary to design the thruster, the electronic system, and the experimental arrangement to meet all the required specifications. To the author's knowledge, this marks the first time a water resistojet is being tested in a zero-g flight campaign.

II. Water Electrothermal Thruster

A significant issue with using liquid water as a propellant is its tendency to fluctuate in microgravity. The design of the vaporization chamber must address this problem, as the uncontrolled movement of non-vaporized water within the chamber can result in some of it reaching the outlet without undergoing vaporization. Consequently, liquid water could enter the nozzle, thereby diminishing performance and wasting propellant. Furthermore, the boiling process in microgravity conditions differs markedly from the vaporization process observed on Earth. This discrepancy can lead to variations in performance between laboratory measurements and actual orbital conditions.

A. State of the Art

Over the last decades, using water as propellant for resistojets has been explored extensively. NASA Lewis conducted research on liquid-water resistojets from 1987 to 1993, although the program was terminated before any prototypes could undergo flight testing. Subsequently, Rocketdyne and Technion collaborated on a multipropellant resistojet project, examining operational characteristics with fluids like hydrogen, helium, methane, water, nitrogen, air, argon, and carbon dioxide. Data were collected for two thruster configurations: one featuring a vaporization chamber, and the other using the nozzle itself as the vaporizer. The decoupled system, using a separate vaporization chamber, behaved similarly to other tested propellants, achieving a

maximum specific impulse (I_{sp}) of 184 seconds and 230 mN thrust. Power consumption was 466 W for the vaporization chamber and 692 W for the main thruster. In contrast, the coupled system, functioning as both vaporizer and superheater, operated at higher temperatures with significant temperature gradients, leading to rapid vaporization of liquid water and a mix of vapor and droplets in the nozzle. This configuration produced 84 mN thrust at 289 W, with the nozzle heater reaching about 870 K. Ensuring efficient contact between liquid and solid phases in microgravity remains a key challenge for electrothermal vaporizing thrusters, impacting overall performance. Various solutions have been proposed over the years to address this issue.[5]

1. **SWIRL FLOW BOILER** To enhance vapor drying, the two-phase mixture is often swirled within the boiler, centrifuging the liquid towards the heated wall where it vaporizes efficiently.
2. **CROSS FLOW HEAT EXCHANGER** The two-phase flow traverses a series of heated tubes where the liquid makes contact and undergoes vaporization.
3. **ROTATING BOILER** A rotating vaporization chamber system offers several benefits: it operates independently of gravitational fields and orientation. Centrifugal forces within the vapor space yield vapor with low moisture content (high quality), maintaining a stable liquid-vapor interface for consistent flow. However, the system moving components increase construction and implementation complexity.
4. **POROUS MEDIUM BOILER** Porous materials or packed-bed heat exchangers effectively vaporize liquids, similar to cross-flow heat exchangers.[7,8]

Recent advancements have seen the emergence of diverse water vaporizing thrusters from global research institutions and companies. For instance, at the University of Tokyo, a thruster with a vaporization chamber and multiple nozzles operates at a low pressure of 100 kPa inside the tank. Nozzles designed for attitude control have a throat diameter of 1.2 mm, while those for orbit change maneuvers measure 2.6 mm. This thruster achieves stable operation, producing 1.6 mN of thrust and a specific impulse (I_{sp}) of approximately 70 seconds.[1,2,10]

In another development, the French startup ThrustMe has developed an electrothermal water vapor thruster with a vaporization chamber. Test results demonstrate its capability to achieve a specific impulse exceeding 100 seconds and a thrust of 2 mN, operating at a chamber temperature of $50°C$ with a nozzle throat diameter of 0.4 mm.[3] Meanwhile, Japanese company Pale Blue is developing various types of water-based thrusters, including three types of resistojets. According to their specifications, these thrusters have a power range between 6.5 W and 50 W and produce a thrust ranging from 1 mN to 10 mN.[12] Lastly, Finland-based Aurora company has engineered a water-fueled micro-resistojet specifically designed for collision avoidance applications.[13]

B. Thruster Overview

Figure 1 depicts a schematic diagram of the water resistojet, designed at the ICARE laboratories of CNRS in Orléans. The operation of the thruster is relatively straightforward. Pressurized water is in liquid state within the upper shell of the spherical tank. When the valve (V1) is opened for a certain period of time, a quantity of liquid water is injected into the vaporization chamber. Water boils on the heated walls of the vaporization chamber. The temperature of the walls is controlled by the control system.

Once the saturation pressure is achieved, the valve (V2) can be opened to release the vapor. As long as there is liquid water in the vaporization chamber, the pressure will remain at the saturation pressure. The water vapor flows into the nozzle, where it is superheated to increase the specific impulse I_{sp}.

It is crucial to minimize the pressure losses between the vaporization chamber and the nozzle because the thrust is directly proportional to the total pressure before the convergent section of the nozzle.

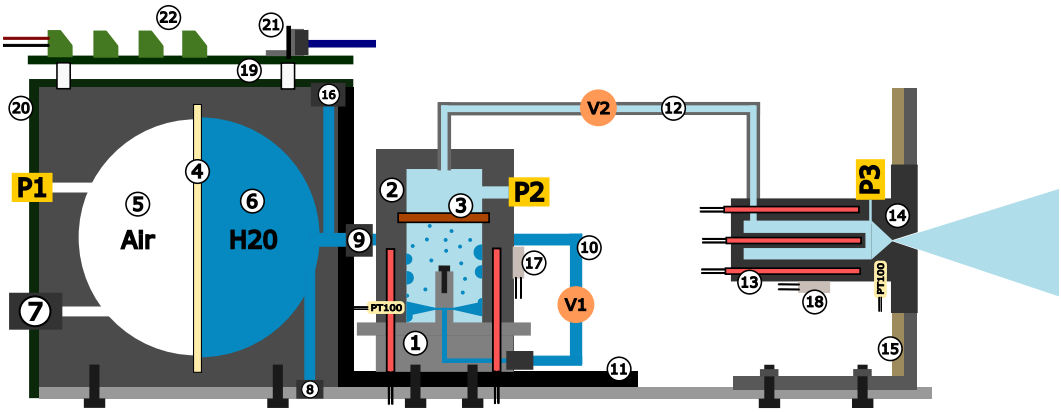

Figure 1. Resistojet Schematic

1. Injector
2. Case
3. Copper Metallic Foam
4. Elastic Membrane
5. Air Compartment
6. Water Compartment
7. Air Filling Valve
8. Water Filling Valve
9. Swagelok Tube Fitting
10. PTFE Tube
11. ABS Support
12. Stainless Steel Tube 1/4 in
13. Heater (28 V)
14. Nozzle Case
15. PEEK Support
16. Vent Valve
17. Thermal Cut Off (55°C)
18. Thermal Cut Off (85°C)
19. PCB Connectors 1
20. PCB Connectors 2
21. Sub D-9 Connector
22. Screw Terminals

C. Spherical Tank

Design of the tank for storing water in its liquid state posed significant challenges. The tank required specific characteristics to handle the liquid propellant. There are mainly two types of tanks for liquid fuels used in space applications: capillary tanks and tanks with a bladder. For the resistojet, we opted for a bladder tank due to its easier implementation. In microgravity, the liquid propellant may not always remain in contact with the tank outlet section unless an elastic membrane between the pressurizing gas and the liquid constantly pushes it toward the outlet. Finding a low-cost, effective membrane was challenging. Due to our lack of experience with this technology, we built a spherical test tank in transparent acrylic (PMMA). This enabled us to visually confirm the membrane correct operation. The tank consists of two spherical caps made of transparent acrylic PMMA. A 2 mm thick elastic membrane, also serving as a gasket, is positioned between them. The two caps are secured together with 15 M2 bolts that pass through both the caps and the bladder, as can be seen in Figure 2.

To install Swagelok-type pipe fittings, aluminum inserts were fabricated and bonded into designated holes using vacuum-compatible adhesive, and the entire assembly was sealed with epoxy resin to enhance integrity. The use of inserts was necessary because acrylic is too fragile to be threaded directly.

Before operation, the lower compartment of the tank is filled with air at atmospheric pressure, serving as pressurizing gas. The upper compartment, however, filled with distilled liquid water. To fill the tank with water, a 35 ml syringe pump was used. Additionally, to vent the air during the filling process, a separate side vent hole was provided. It's worth noting that another spherical tank, made of aluminum and featuring the same membrane, was fabricated for microgravity testing purposes. This decision was taken because the

solution involving bonded metallic inserts was not sufficiently reliable. However, the transparent acrylic tank played a crucial role in understanding the functionality of the elastic bladder.

Figure 2. Acrylic transparent spherical tank with an elastic bladder.

D. Vaporization Chamber

The vaporization chamber was machined from aluminum 6082. This material was chosen for its ease of machining, low cost, and relatively high thermal conductivity ($220\frac{W}{m\cdot K}$). As shown in the Figure 1 and Figure 3, the vaporization chamber is assembled from two parts: a case and an injector. The injector houses a Lee Company cartridge solenoid microvalve, operating at 12 V (LFNA1250125H). Moreover, it includes a NPT 1/8 port for accommodating a Swagelok adapter, enabling connection to the inlet tube. Pressurized liquid water is expelled from the injector, spraying against the case's wall. the wall is kept at a precise temperature by the control system. The water exits the injector through four apertures, ensuring maximum contact between the liquid and the heated surfaces. The casing is divided into two compartments: one with a volume of 32 cm^3 where the water is vaporized, and the other where the vapor is expelled. Between these compartments, a sheet of copper metal foam has been installed, with a thickness of 4 mm and an average pore size of 1.5 mm. The metal foam acts as a filter for the liquid droplets, which, in the absence of gravity, might not stay in contact with the heated surfaces of the vaporization compartment. This prevents liquid water from reaching the nozzle without first being vaporized.

The vaporization chamber is heated by three cartridge heaters, each rated at 28V and 20 Watts, with a diameter of 1/8 inch. The heaters are inserted into designated holes machined into the case of the vaporization chamber. To enhance thermal conductivity between the heaters and the chamber, a boron nitride thermal paste has been applied. for a rapid response from the temperature control system, PT100 sensors have been positioned as close as possible to the chamber internal walls where the water boils. The solenoid valve has a maximum operating temperature of 50 °C. For safety reasons, two thermal fuses rated at 55 °C each have been installed near the valve. An Honeywell pressure transducer has been installed on the case to monitor the saturation pressure of the vapor.

The power balance of the vaporization chamber is described by Eq(1). The total input power comprises the power required for vaporization, the power for superheating in the nozzle, and any radiative and conductive power losses. The vaporization power, assuming we are in the nucleate boiling regime, can also be expressed by the Eq(2), where A_l is the liquid contact area, T_{wall} is the wall temperature, and T_{sat} the saturation temperature at the pressure in the vaporization chamber. The values of the exponent n and the proportionality constant C depend on the inclination of the surface, the geometry, the system pressure, the surface roughness, and other factors such as the gravity level.[6]

To minimize conductive power losses, the aluminum vaporization chamber is mounted on an ABS support, which is directly connected to the tank. Additionally, the tube that carries liquid water from the tank to the vaporization chamber is made of PTFE, further reducing thermal power losses, as shown in Figure 1 and Figure 5.

$$P_{in} = \dot{m}h_{vl} + P_{superheat} + P_{cond} + P_{rad} \tag{1}$$

$$P_{vap} = \dot{m}h_{vl} = A_l C(T_{wall} - T_{sat})^n \tag{2}$$

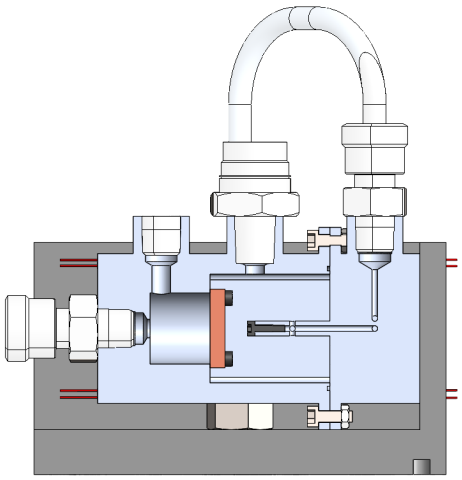

Figure 3. 3D CAD Drawing: Vaporization Chamber.

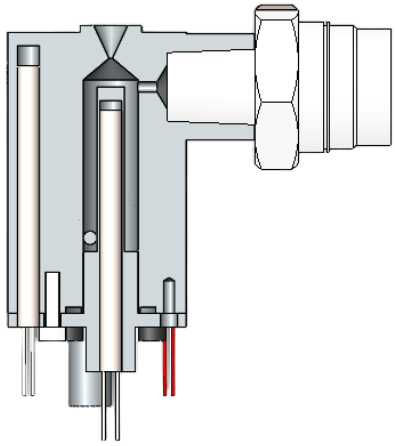

Figure 4. 3D CAD Drawing: Nozzle.

E. Nozzle

The nozzle is made of stainless steel to withstand elevated temperatures. It is heated by three 20-watt cartridge heaters, each operating at 28V. It consists of two components: an outer casing and an inner insert that creates an annular channel. One heater is located inside the insert, while the other two are embedded in the outer shell, as illustrated in Figure 4. This arrangement ensures that all metal surfaces in contact with the fluid are adequately heated. The nozzle features a conical convergent-divergent design with a throat diameter of 0.5 mm and a nozzle area ratio of 25.

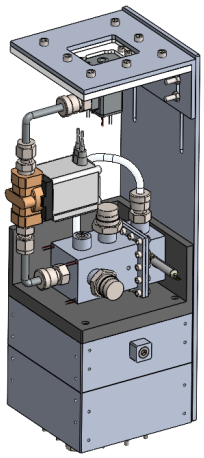

Figure 5. 3D CAD Drawing: Resistojet Assembly.

III. Zero-G Flight Experiment

The experimental flight campaign (VP177) took place in late March 2024 at the Bordeaux-Mérignac Airport (France). The parabolic flight campaign was organized by Novespace, a joint-stock company con-

trolled by the French Space Agency (CNES). Novespace mostly arranges flights for researchers selected by the CNES, The European Space Agency (ESA), or the German Aerospace Center (DLR).

The experimental campaign spanned two weeks. During the first week, Novespace's technicians and engineers thoroughly inspected the experimental apparatus, ensuring it met all safety requirements. The apparatus was then installed on the aircraft, interfaced with the onboard electrical system; and tested to verify proper functionality.

In the second week, three experimental flights were carried out over three consecutive days. Each flight performed 31 parabolas, totaling 93 parabolas for the entire week. The Figure 6 illustrates the profile of a typical parabolic flight maneuver. As shown, the microgravity phase, which lasts approximately 22 seconds, is preceded and followed by phases of hypergravity (1.8-g). The thruster was tested under normal gravity (1-g), microgravity, and hypergravity (1.8-g) conditions to assess if there were any variations in performance.

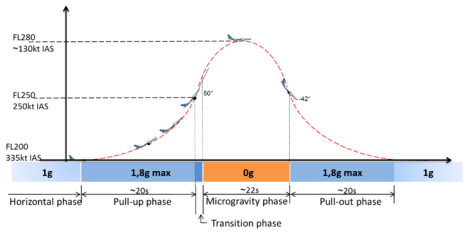

Figure 6. Parabolic Maneuver Profile..

Figure 7. Airbus 310 Zero G.

A. Experimental Equipment Fixation

The experimental equipment must be securely fastened to the aircraft during an experimental flight. Novespace, the organizing entity for the flights, furnishes comprehensive documentation on the experimental structure design to ensure compliance with safety requirements. Every device and piece of equipment must be mounted on frames called racks, each of which must adhere to predefined dimensions and be built with appropriately resistant components.

The design of the rack also needed to account for its orientation within the aircraft. Novespace mandates that the structure must withstand an acceleration of 9 g along the direction of the cockpit (x-axis). Each rack has a weight limit that must not exceed 200 kg. Therefore, it was necessary to build two racks for this experiment to accommodate all the components.

The frame of the structure was assembled using Bosh 45x45 aluminium profiles, secured together with 45x45 brackets along the y and z directions (roll and yaw axis respectivily). Along the x direction, more robust 45x90 brackets were used to withstand the higher 9g accelleration. Although passangers and equipments on board do not normally experience such high acceleration during regular operation, in case of failure, it is essential that all components are securely fixed. The Bosh profile frame of the two racks is attached to a 10 mm tick aluminum plate using additional brackets. This baseplate is then bolted to the aircraft floor with special M10 bolts.

The center of gravity of the racks must be kept relatively low to prevent excessive loads on the bolts securing the aluminum plate to the aircraft rails. Each edge of the structure was covered with 19 mm thick fireproof foam to prevent onboard operators from hitting the sharp metal edges during parabolic flight phase. To reinforce the structure, 5 mm aluminum plates were added to each corner of the frame (Gussets), as can be seen in Figure 8.

Every bolt was tightened with a torque of 25 N·m, and each was marked with red ink to check for any loosening. Additionally, thread-locking adhesive was applied.

To determine the weight and dimensions of each individual components, as well as the position of the structure center of gravity, each component was meticulously design using a CAD drawing software. As mentioned earlier, two racks were fabricated for this experiment. Below, detailed information regarding these two structures, including their actual dimensions and images, will be provided.

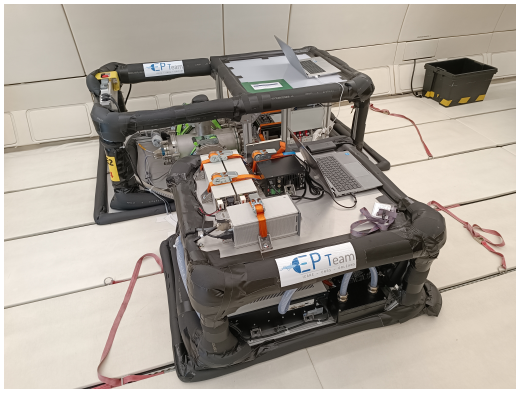

Figure 8. Photograph of the experimental apparatus on the aircraft.

1. Rack 1

Rack 1, the primary rack, has dimensions of 800 mm along the y-axis and 1500 mm along the x-axis. The frame is assembled from Bosh longitudinal profiles and vertical profiles called uprights. Each upright must be in contact with the baseplate to ensure the structure's stability. The height of the frame is 500 mm, and it is partially covered by a polycarbonate plate that supports one of the two laptops used in the experiment. As shown in Figure 9. To keep the center of gravity low, all heavy components are positioned directly on the baseplate. The vacuum chamber consists of two components: a cross-type vacuum chamber with a diameter of 200 mm made of stainless steel, and a T-section of the same diameter and material, as shown in Figure 11.

The entire vacuum chamber assembly is supported by seven plates called clamps, each 10 mm thick and made of aluminum 5083. One side of each clamp has been machined into a cylindrical shape to ensure a precise fit and adherence to the vacuum chamber. These clamps are anchored to the baseplate with standard Bosh brackets, preventing movement along the x and y axes. Movement along the z-axis is restricted by high-strenght straps, secured to the baseplate with stainless steel eye bolts. The straps; each with a capacity of 1100 kg, are tightened around the vacuum chamber to ensure stability.

Additionally, an oscilloscope is anchored to the baseplate of the rack. The oscilloscope is used to measure the current in the heaters positioned in the vaporization chamber and the nozzle. On one side of the frame, two additional uprights are installed to support two fireproof ABS boxes. These boxes house the printed circuit boards necessary for thruster control and data acquisition, see Figure 9.

The total weight of the rack 1 is 190 kg, slightly below the imposed limit of 200 kg. Therefore, all additional components required for the experiment have been allocated to a separate rack.

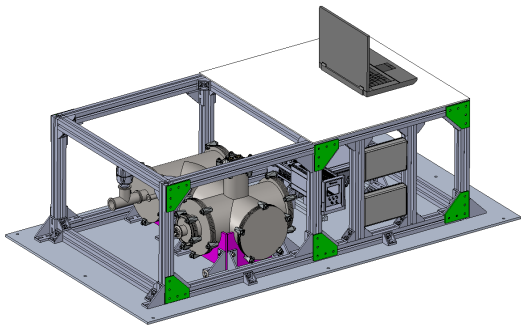

Figure 9. 3D CAD Drawing: Rack 1. (Gussets in green and clamps in magenta).

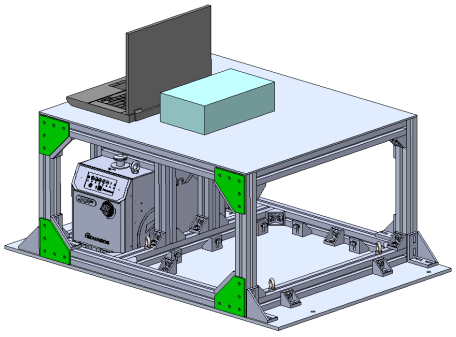

Figure 10. 3D CAD Drawing: Rack 2.

2. Rack 2

Rack 2 is smaller in size compared to rack 1, measuring 800 mm along the x-axis, 800 mm along the y-axis, and 450 mm in height. The frame is anchored to the aircraft floor using a 100 mm thick aluminum baseplate. The plate supports the primary pump, which has been enclosed in a cage constructed from Bosch profiles. Due to the significant weight of this component, structural calculations were necessary.

A 5 mm thick aluminum plate has been installed on the top of the structure. The top plate supports a power supply capable of delivering of a maximum of 10 A at 60 V, along with two twin power supplies required for operational amplifier circuits demanding a dual voltage of +- 15V. It also withstands the electronic controller for the primary pump as well as the pressure reader connected to the vacuum chamber's pressure sensor.

Each component movement along the x and y axes is restricted by 45x45 Bosh brackets, while 300 kg capacity straps have been installed to prevent movement along the z-axis, as exemplified in Figure 10 and Figure 8.

It was not feasible to connect the primary pump's exhaust to the aircraft's ventilation system due to the risk of water freezing in the line. Consequently, it was decided to vent the gases directly into the cabin. To prevent water from coming into contact with the operators, a filter was placed between the pump's exhaust and the cabin. A stainless steel box was procured and filled with absorbent material. Two 22 mm diameter holes were drilled into the box to accommodate fittings for the exhaust hose from the pump and the actual discharge pipe. This setup ensures that any liquid water in the exhaust is absorbed before the gases are released into the cabin.

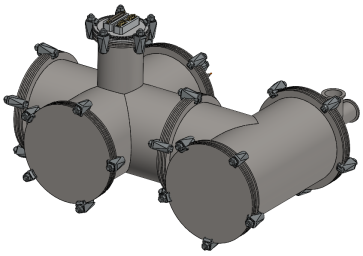

Figure 11. 3D CAD Drawing: Vacuum Chamber Cross Section.

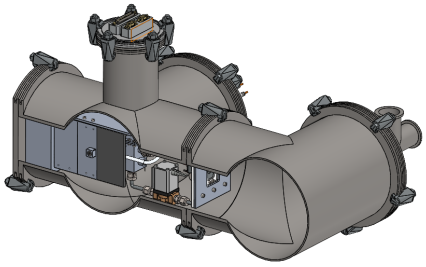

Figure 12. 3D CAD drawing: Vacuum Chamber Cross Section.

B. Electrical System

To control the thruster and read parameters such as pressure and temperature, two printed circuit boards were developed. Initially, these circuits were designed to be placed inside the vacuum chamber, directly installed on the thruster. This would have significantly reduced the number of electrical cables leaving the thruster, thereby simplifying thrust measurement. However, due to the stringent safety requirements and space constraints, it was decided to redesign the printed electronic circuits to operate outside the vacuum chamber.

The transition of the cables from inside to outside the chamber was achieved using a Plug-in flange containing an 8-pins high-current (41 ampere maximum) pass-through used for heater's current and 2xSub-D9 pass-throughs for sensor signals, such as pressure sensors and PT100s, as well commands for solenoid valves. For this experiment, two printed circuit boards (PCBs) were designed: one to regulate the current in the heaters and control the the solenoid valves, and another to read parameters such as pressure, temperature, and accelleration. The design process employed KiCad,[4] an open source software widely used for creating printed circuit boards with a high number of layers, see Figure 13 and Figure 14. Given the simplicity of the electronic components used in these circuits, they were designed with only two layers to minimize costs and manufacturing time. Each PCBs includes an Arduino Nano microcontroller directly mounted on it. The microcontrollers were programmed in C++ using the Arduino IDE software. A detailed description of the two electronic circuits will follow. The decision to fabricate printed circuit boards (PCBs) rather than simple homemade circuits with soldered components was driven by the desire for a safer and more reliable solution that avoids the excessive use of electrical wiring. The current in each PCB trace was carefully calculated,

and the trace widths were designed to adequately handle the specified current. A safety factor of 1.5 was applied in determining the trace dimensions.

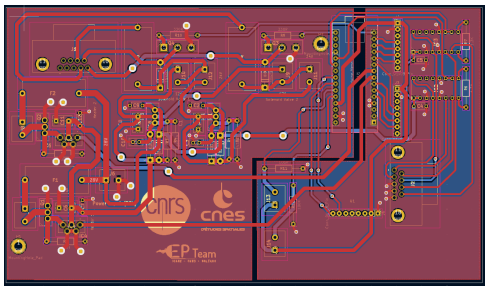

Figure 13. Printed Circuit Board 1: KiCad Schematic

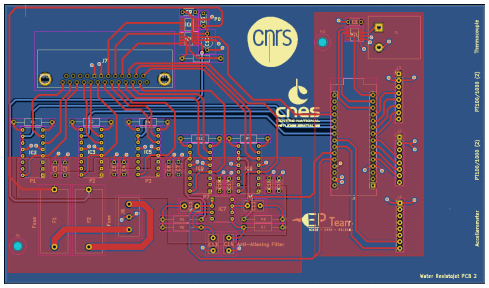

Figure 14. Printed Circuit Board 2: KiCad Schematic

1. Printed Control Board 1

The printed circuit board 1 operates with an input voltage of 28V, the same input voltage used to power the cartridge heaters located inside the vaporization chamber and nozzle. The solenoid valves operate at relatively low voltages of 24 V and 12 V, requiring the design of two voltage regulator circuits using the LM338T linear voltage regulator.

To independently control the temperature of the vaporization chamber and the nozzle, two separate control circuits have been implemented on the board. These circuits function in the same manner and utilize identical components. The heaters are connected in parallel, ensuring they always receive a voltage of 28 volts. The current through the heaters is regulated by a MOSFET (IRFB4115PBF), which in turn is controlled by a MOSFET driver driven by the microcontroller (Arduino Nano). The microncontroller sends a PWM signal to the MOSFET driver (MCP1507). The PWM signal is generated by the PID control code written in the Arduino IDE and uploaded within the microcontroller. For precise and accurate temperature readings, PT100 sensors were used. A PT100 is a temperature sensor that changes its resistance in response to temperature variations. Since the resistance change is often very small, amplification is required. Therefore, two integrated circuits capable of amplifying and reading the signal from the PT100 sensors were installed on the board (MAX31865). The solenoid valves are controlled by transistors that receive signals directly from the microcontroller. Fuses are installed upstream of the heater and solenoid valve circuits, opening the circuit in case of excessive current draw. The PCB has been designed with two layers, red and blue, as shown in the Figure 13. The traces carrying the current for the heaters have been made larger to prevent overheating issues.

2. Printed Control Board 2

The second electronic board is shown in the Figure 14; it is dedicated to the acquisition of pressure, temperature and acceleration data. It contains three integrated electronic circuits composed of operational amplifiers, arranged in a configuration known as an instrumentation amplifier, which read and amplify the output signal from the pressure sensor.

The pressure sensors used have a maximum output signal of 100 mV, which must be amplified and stabilized to be read by the microcontroller board (Arduino Uno). The controller is directly connected via a USB port to one of the two laptops, and data acquisition and storage are carried out using Excel Data Streaming with a sampling time of 150 ms.

The board also includes two amplifiers (MAX31865) for reading the PT100 signals. To measure the relative acceleration onboard we used an ADXL345 low power, 3-axis accelerometer, connected to the microcontroller through an SPI interface.

3. PCB Connectors

To simplify the connection of electrical cables within the vacuum chamber, two interface circuit boards were designed. These boards feature a 9-pin and a 25-pin sub-D connector, respectively, making it straightforward

to connect and prepare the thruster inside the vacuum chamber. Because these two boards need to operate in a vacuum environment, they were designed with wider traces to avoid overheating problems, see the Figure 15 and Figure 16. All electronic boards, including the control PCBs, were manufactured to aerospace-grade quality standards. The base material used is FR-4, with a copper layer thickness of 1 oz.

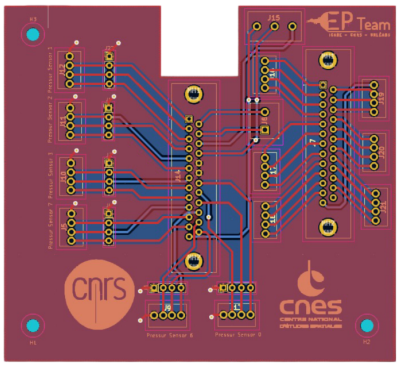

Figure 15. PCB Connector 1

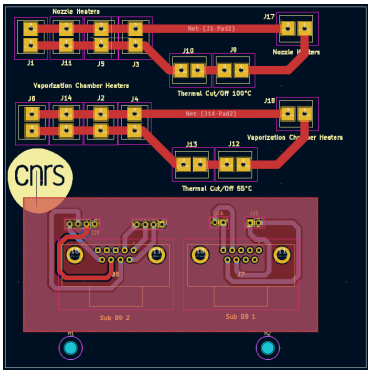

Figure 16. PCB Connector 2

4. Experimental Setup

The diagram in Figure 17 illustrates the entire experimental setup. The thruster is directly mounted to the vacuum chamber flange using an aluminum support. Four threaded holes are drilled into the flange to accommodate M6 screws that secure the support. Pressure inside the vacuum chamber is monitored by a vacuum pressure gauge. During engine operation, the back pressure was of 8.50E-01 mbar. Between the primary pump and the cabin, there is a box filled with absorbent material that serves as a filter for liquid water. Two current probes attached to an oscilloscope are clamped to the cables carrying current to the heaters in the chamber and nozzle, respectively. The two electronic boards are connected via USB cables to two laptops used in the experiment. One laptop controls the Resistojet and regulates its temperature, while the other is dedicated to data acquisition. The primary pump is an Edwards nXR40i, which weighs 28 kg and has a peak pumping speed of 40 m^3h^{-1}.

1. Water Trap
2. Sub-D 25 feedthrough
3. Vacuum pressure gauge
4. Sub-D 9/high current
5. Thruster support
6. Vacuum valve
7. Primary pump
8. Heater driving circuit (1)
9. Heater driving circuit (2)
10. Valve (V1) driving circuit
11. Valve (V2) driving circuit
12. Voltage regulator (24V)
13. Voltage regulator (12V)
14. MAX31865
15. Heater power supply
16. Twin power supply
17. Pressure sensors circuit
18. ADXL345 accelerometer
19. Arduino Nano
20. Current probe

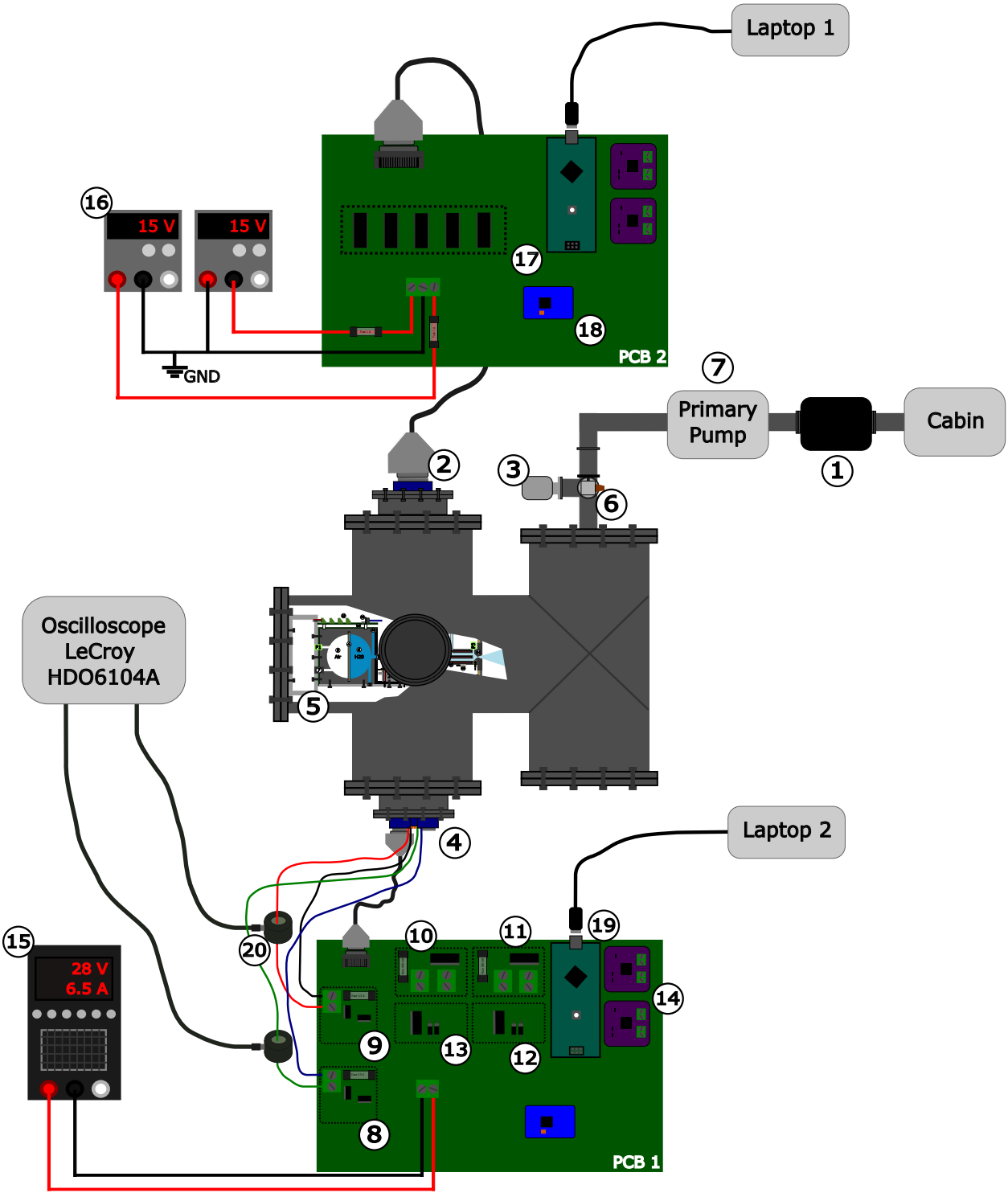

Figure 17. Experimental Setup

IV. Results

Throughout the entire experimental campaign, the following parameters were measured: pressure, temperature, and acceleration. Figure 18, Figure 19 and Figure 20 show the measured quantities across all three days of flights. In the first day, it was decided to perform only one pulse each parabola, meaning the second solenoid valve was left open throughout. During the initial 16 parabolas, the thruster was activated solely during the microgravity phase. In the last ten parabolas, water was injected both during the microgravity phase and when the aircraft was in a steady-state motion following the 1.8-g gravity phase.

The vaporization chamber temperature was maintained relatively constant by the control system, ranging between 52.5 °C and 54.5 °C. The vaporization chamber pressure showed an increasing trend during the initial parabolas before stabilizing at a nearly constant value of 130 mbar. This increasing trend was also observed on the 27th and 28th.

In the Figure 21, we can see a zoomed-in view of 5 parabolas. As observed, the impulses at 1-g and 0-g do not exhibit significant differences in shape. As evident, there are no significant differences in the pressure values between the zero gravity and normal gravity conditions. However, it is noteworthy that the chamber pressure shows significant oscillations when the thruster is not generating thrust, i.e., when the liquid water in the chamber should have fully vaporized. Believing that the cause of these oscillations was the pressure sensor, it was replaced, but the oscillations persisted. A possible explanation for this could be attributed to the fact that liquid water may condense on the pressure sensor.

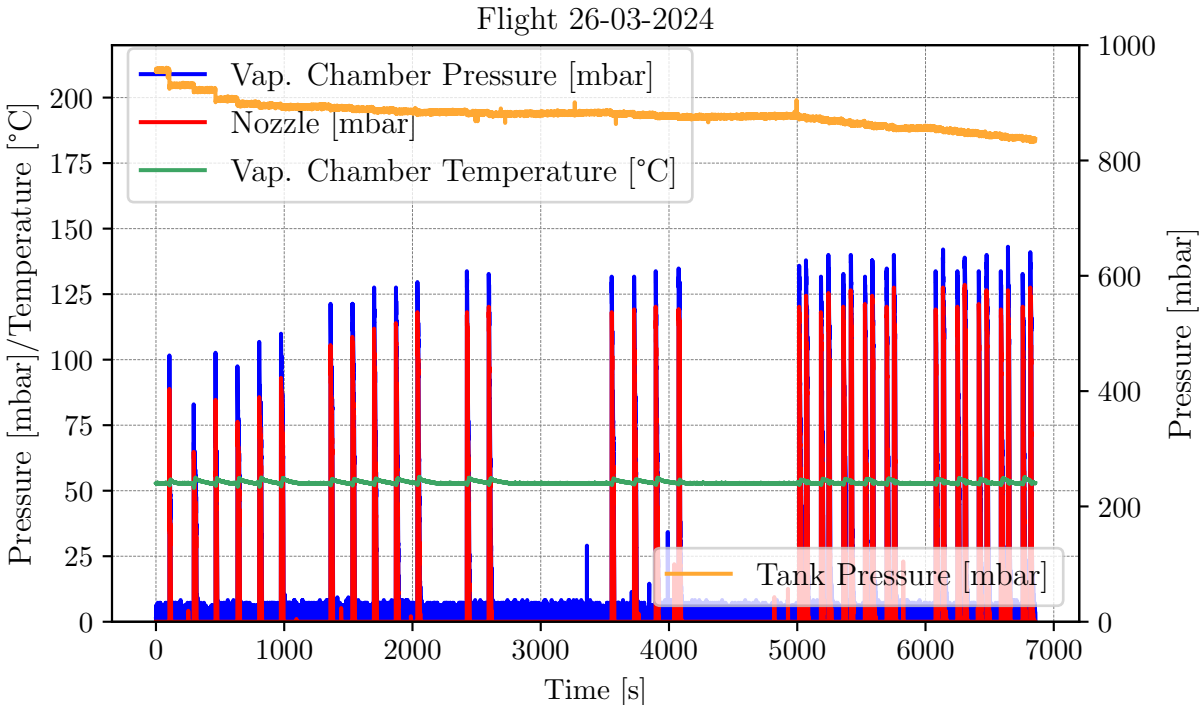

Figure 18. First Flight Experimental Data (26-03-2024).

The power has been measured indirectly by monitoring the current in the heaters. Given that the load is purely resistive, the instantaneous power required to maintain the vaporization chamber at the desired temperature was calculated using the Eq 3. A current probe with a bandwidth of 100 MHz and a maximum current measurement capacity of 30 A was employed for this purpose.

$$P(t) = i(t)^2 \cdot R_{parallel} \tag{3}$$

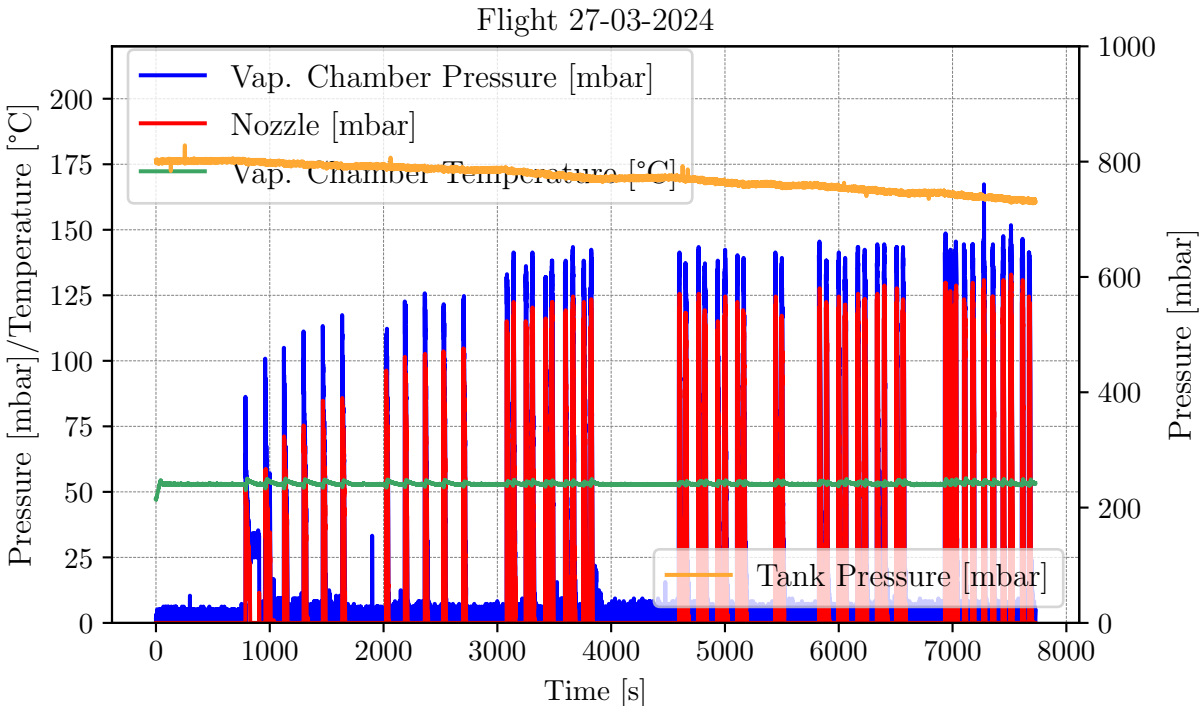

Figure 19. Second Flight Experimental Data (27-03-2024).

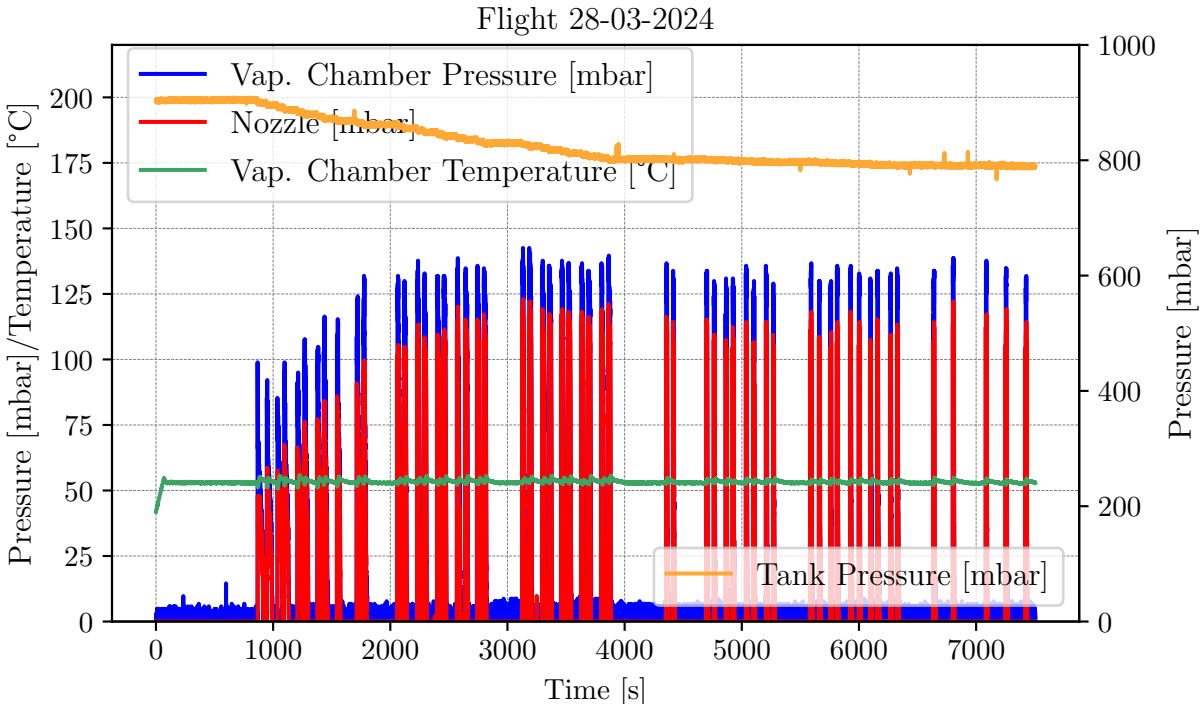

Figure 20. Third Flight Experimental Data (28-03-2024).

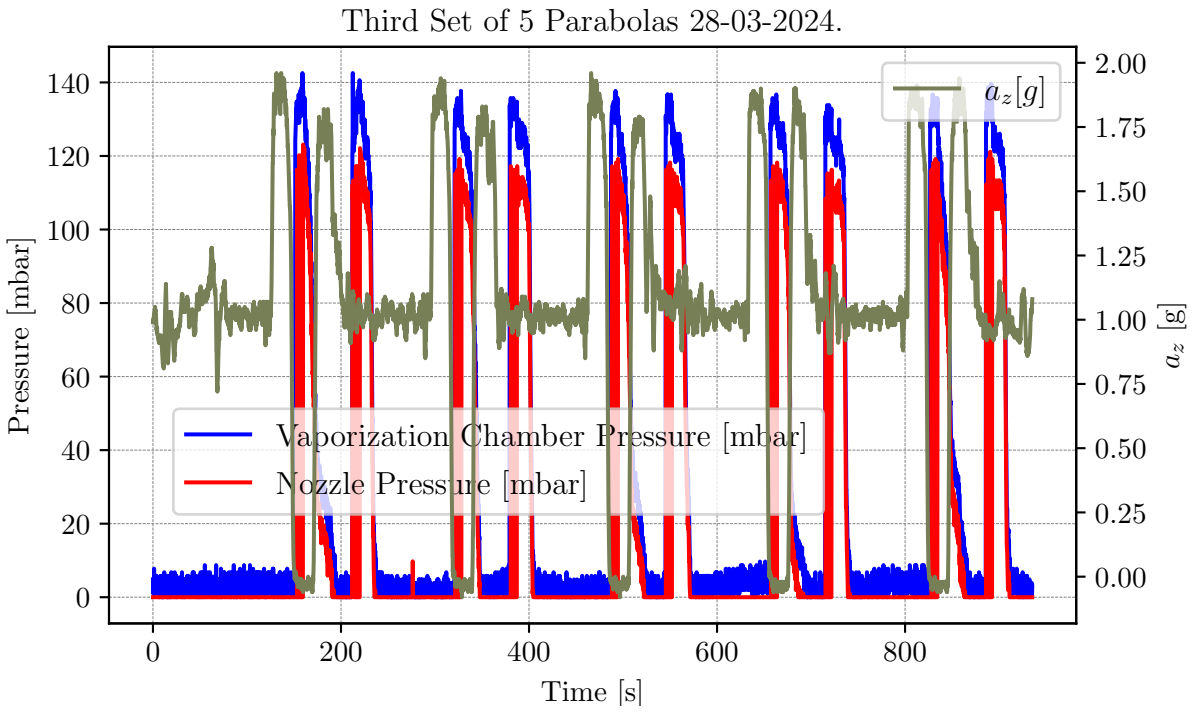

Figure 21. 5 Parabolas: water injection at 0-g and 1-g.

The current was measured for each parabola. A second current probe was used to set a trigger on valve V1; when this valve opened, the oscilloscope began recording the current supplied to the heaters. The recording interval was set to 50 seconds: 10 seconds before the pulse sent to valve V1 and 40 seconds after it. This approach allowed for the measurement of power throughout the entire microgravity interval and for the duration that water was boiling within the vaporization chamber.

Figure 23 illustrates the typical behavior of instantaneous power during a parabola. As observed, immediately after the valve pulse at time $t = 0$, the temperature of the vaporization chamber walls drops below the reference value because the water cools the chamber walls, see Figure 22. The control system responds by supplying more current to the heaters to restore the vaporization chamber temperature to the desired level.

The time-averaged power over the 50-second interval ($\Delta t = 50s$) has been computed for each pulse using the Equation 4. The average power values of the second flight (27-03-2024) are presented in Table 1.

The average power at 1-g appears to be slightly lower than that calculated at 0-g. This could be due to the fact that the initial temperature of the vaporization chamber walls in the 1-g case is always slightly higher, as the system has not had sufficient time to reset to the desired temperature between the microgravity and 1-g phases. Another reason could be attributed to the fact that in microgravity, the heat transfer nucleate boiling coefficient can be lower compared to the case of normal gravity.[9,11] It should also be noted that the amount of water injected into the chamber is not exactly the same each time, as the tank pressure decreases over time.

$$< P(t) >_{\Delta t} = \frac{1}{\Delta t} \int_{\Delta t} P(t)dt \tag{4}$$

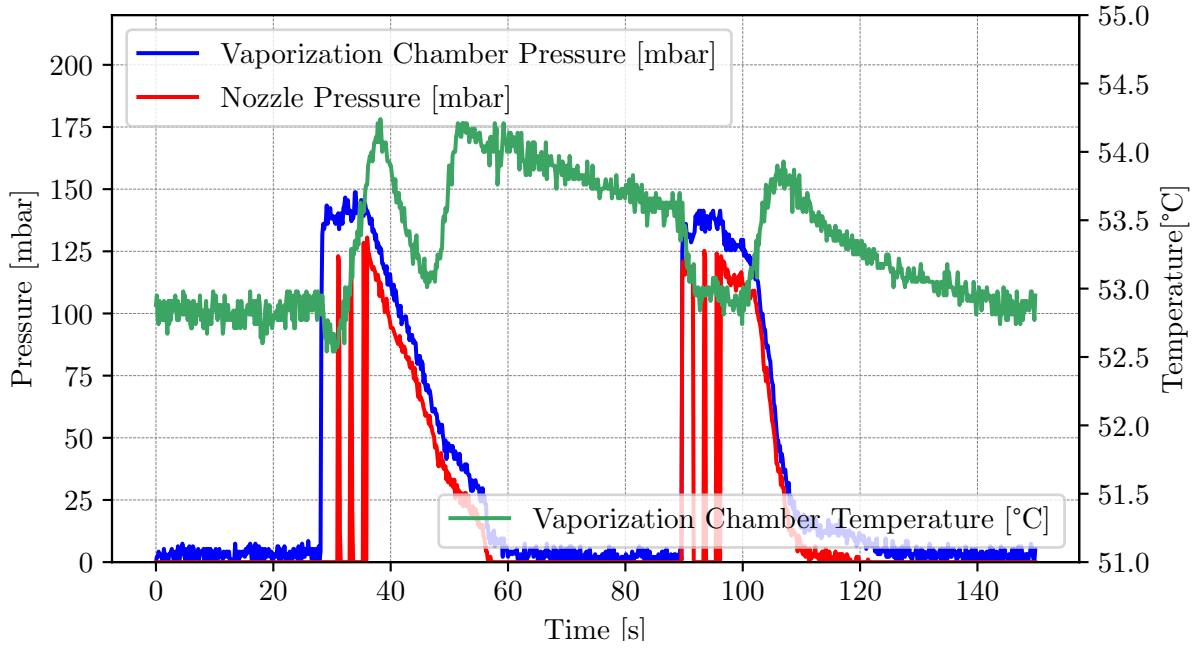

Figure 22. Two impulses at 1-g and 0-g.

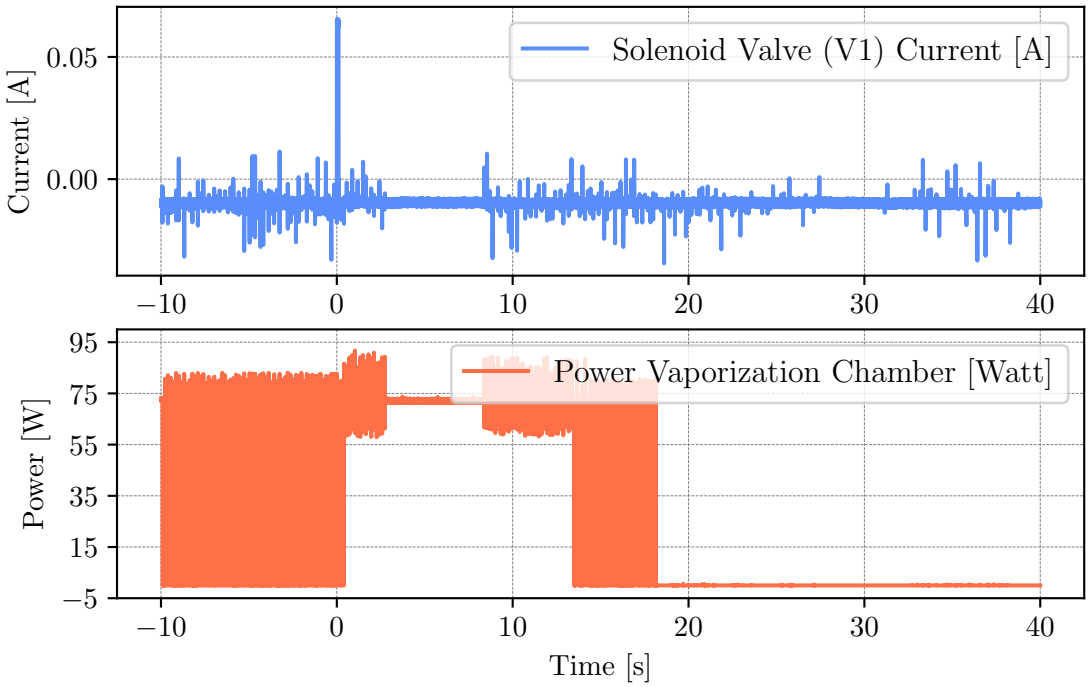

Figure 23. Valve Impulse, Power

Parabola N°	0-g Average Power [W]	1-g Average Power [W]	1.8-g Average Power [W]
1	21.7	13.9	/
2	22.0	12.1	/
3	22.2	11.5	/
4	19.2	15.1	/
5	/	/	/
6	14.5	18.0	/
7	15.2	17.4	/
8	15.6	14.7	/
9	16.5	15.3	/
10	17.7	15.3	/
11	14.5	15.4	/
12	16.5	16.6	/
13	14.3	17.1	/
14	14.3	15.1	/
15	11.5	19.3	/
16	15.6	15.4	/
17	10.5	1.7	/
18	10.7	6.5	/
19	8.2	4.0	/
20	10.9	5.0	/
21	10.0	7.4	/
22	8.5	7.0	/
23	10.0	3.4	/
24	9.8	8.0	/
25	8.0	2.1	/
26	9.8	6.2	/
27	/	/	10.9
28	/	/	10.4
29	/	/	9.3
30	/	/	8.3
31	/	/	8.9

Table 1. Average Power at 0-g, 1-g and 1.8-g.

V. Conclusion

In this paper, we described the design of a water Resistojet developed over the past year at the ICARE laboratories of CNRS in Orléans. Additionally, we presented the experimental setup used during the March 2024 flight campaign at Bordeaux Mérignac Airport in France. The entire structure was built from scratch, including the electronic control system and data logging. Throughout the design phases, we encountered numerous challenges due to the author limited experience in conducting these kind of experiments. Moreover, due to stringent safety requirements, the Resistojet design had to undergo modifications. Pressure, temperature, and power were measured during microgravity, normal gravity, and 1.8-g phases. Pressure curves showed no significant differences between 1-g and 0-g cases, while power consumption for vaporization appeared slightly higher in 0-g conditions. It's worth noting that this was a preliminary attempt to measure flight performance. Further flight campaigns are necessary to deepen our understanding of the thruster's operation in microgravity. For instance, a beneficial step would be to incorporate a vaporization chamber with a transparent window to observe water vaporization inside. Another crucial improvement to implement in upcoming flight campaigns is the inclusion of a turbomolecular pump. The current chamber pressure of 8.50E-01 mbar during thruster operation is too high to obtain accurate measurements of absolute performance.

Acknowledgments

The experiment has been selected in the CNES parabolic flight campaign (VP177) and it has been financially supported by the French Space Agency (CNES) under grant agreement 262757 and 284001. Sincere thanks are also due to Novespace for their invaluable support, which was crucial to the experiment success. Special recognition goes to Frédéric Gai, who diligently assisted the author throughout the year-long preparation period. Additionally, The author extends sincere thanks to the entire electric propulsion team in Orléans, under the leadership of Stéphane Mazouffre, for their precious support.

References

[1]Jun Asakawa, Hiroyuki Koizumi, Keita Nishii, Naoki Takeda, Masaya Murohara, Ryu Funase, and Kimiya Komurasaki. Fundamental ground experiment of a water resistojet propulsion system: Aquarius installed on a 6u cubesat: Equuleus. *Transactions of the Japan Society for Aeronautical and Space Sciences, Aerospace Technology Japan*, 16(5):427–431, 2018.

[2]Jun Asakawa, Hiroyuki Koizumi, Kazuya Yaginuma, and Yuichi Nakagawa. Pre-flight testing results of multiple water propulsion systems-resistojet and ion thruster for smallsats. 2022.

[3]Fernanda Pimenta Cyrne Giulio Coral Francesco Mattia Bianchi, Elena Zorzoli Rossi. *Proof of concept and preliminary design of a superheated water vapor thruster*. first edition, 2022.

[4]KiCad. Kicad docs.

[5]Timothy J Lawrence. *Research into resistojet rockets for small satellite applications*. University of Surrey (United Kingdom), 1998.

[6]Sandro Manservisi and Ruben Scardovelli. *Termoidraulica dei flussi bifase*. Societá Editrice Esculapio, 2012.

[7]WEARL MORREN. Preliminary characterizations of a water vaporizer for resistojet applications. In *28th Joint Propulsion Conference and Exhibit*, page 3533, 1992.

[8]WEARL MORREN and JAMES STONE. Development of a liquid-fed water resistojet. In *24th Joint Propulsion Conference*, page 3288, 1987.

[9]Keita Nishii. *Experimental study of the multiphase flow inside water thrusters for microspacecraft*. University of Tokyo, 2021.

[10]Keita Nishii, Jun Asakawa, Kosei Kikuchi, Mariko Akiyama, Qihang Wang, Masaya Murohara, Yasuho Ataka, Hiroyuki Koizumi, Ryu Funase, and Kimiya Komurasaki. Flight model development and ground demonstration of water resistojet propulsion system for cubesats. *Transactions of the Japan Society for Aeronautical and Space Sciences*, 63(4):141–150, 2020.

[11]Toshiharu Oka, Yoshiyuki Abe, Yasuhiko H Mori, and Akira Nagashima. Pool boiling heat transfer in microgravity: experiments with cfc-113 and water utilizing a drop shaft facility. *JSME International Journal Series B Fluids and Thermal Engineering*, 39(4):798–807, 1996.

[12]Thruster Space Products Pale Blue—Water, Propulsion. Products - pale blue—water, propulsion, thruster, space.

[13]Aurora Propulsion Technologies. Aurora propulsion technologies.